Proceedings of ASME Turbo Expo 2024
Turbomachinery Technical Conference and Exposition
GT2024
June 24-28, 2024, London, England

GT2024-128955

APPLICATION OF MACHINE LEARNING TECHNIQUES IN CALIBRATION AND DATA REDUCTION OF MULTI-HOLE PROBES

Arman Mirhashemi, Paht Juangphanich, Kenji Miki
NASA Glenn Research Center
Cleveland, OH 44135
Email: arman.mirhashemi@nasa.gov

ABSTRACT

This work presents procedures for implementing machine learning methods into existing algorithms for multi-hole probe calibration and data reduction. It demonstrates that using artificial neural networks (ANNs) can decrease the amount of calibration data needed to achieve a specific calibration uncertainty by over 50%*, while also significantly reducing data reduction times. Instead of surface fitting methods, ANNs are employed. Initially, directional calibration coefficients related to flow angles are computed based on pressure measurements, and then these flow angles serve as input parameters for subsequent ANNs to iteratively define Mach number, static pressure, and total pressure. In an alternative approach, new calibration coefficients directly relate pressure measurements from the five-hole probe to the quantities of interest, thereby eliminating the need for iterative algorithms used in conventional surface fitting methods. This method offers several advantages: an average increase of less than* 1% *in calibration uncertainty for flow angles and a significant reduction in data reduction times to a few seconds on average. Additionally, the methodology is confirmed to avoid both over- and under-fitting.*

NOMENCLATURE

cp Calibration coefficient.
α Yaw angle.
ψ Pitch angle.
P Pressure.
P_t Stagnation (total) Pressure.
P_s Static Pressure.
V Velocicty vector.
Ma Mach number.
$\mathbb{M}$ Machine learning model.
n_h Number of hidden layers.
n_n Number of neurons per layer.
$\mathbb{X}$ Feature vector.
σ Error.
cp Calibration coefficient.

INTRODUCTION

Multi-hole probes, such as five and seven hole probes are proven to be one of the most robust, simple and cost effective instruments to obtain time-averaged three-component velocity measurements [1, 2]. Based on the measurements from 3, 5, or 7 pressure ports on the tip of the probe and by utilizing appropriate calibrations, flow characteristics including flow angles, total and static pressures can be calculated in the flow fields with flow angles up to 75 degrees as demonstrated by several researchers [3–5]. These probes are intrusive flow diagnostic instruments, and thus, probes with diameters as small as 1 mm can be fabricated to minimize possible flow disturbances [6].

A directional probe can be operated in two modes, *yaw-nulling* method and *non-nulling* method. The probe is placed in the flow and yaw is adjusted to obtain similar pressure readings from opposite ports in the *yaw-nulling* method. While the calibration and data reduction can be relatively faster in this method The process of data acquisition is complex and requires very

long settling times for the pressure readings to stabilize. In the *non-nulling* method, the pressure readings from the ports on the probe are related to flow properties of interest using a calibration map. This method requires a large set of calibration data and relatively long data reduction times however, operation of the probe through measurement is much less complex. This work investigates and improves the non-nulling mode of operation for five hole probes.

Probe calibration is generally obtained in an open jet [7] or a closed wind tunnel [8]. Probe is placed in a flow-field with known velocity magnitude and flow direction. At a given Reynolds number, the probe is then pitch and yawed through a range of angles to exceed the range of possible velocity vector orientations in the unknown measurement flow field. For each probe orientation, the pressures from the five holes are recorded [9]. It is important to note that if the flow temperature in the flow field where the pressure will be utilized is similar to the calibration temperature, the Reynolds dependency in the calibration procedure can be reduced to the Mach number dependency. This procedure is usually performed for angle increments of $1-2\,deg.$ for various Mach numbers of interest. This approach may need to be repeated for more than 1000 times to cover the calibration points [10] at a given Mach number. After the probe is calibrated, it can be used to measure the flow properties in an unknown flow-field by measuring the pressure values from the five ports and comparing them to the calibration data. Primary advantage of utilizing the non-nulling method is that the calibration will stay valid as long as the probe tip geometry is intact [11]. Two plane calibrations can be repeated during the life of the probe to further validate the calibration [12].

The differential pressure readings from the calibration data can be reduced to non-dimensional pressure coefficients to construct calibration maps [13]. When the probe is placed in a flow with unknown flow properties, the differential pressure coefficients are calculated based on the pressure measurement and then, the same differential pressure coefficients should be found in the calibration maps [14].

Bryer [15] has assessed some of the earlier general calibration methods and reported the limitations of these models. Dudsinsky and Krause [1] utilized graphical methods to obtain the flow characteristics from calibration maps while Galington [16] used polynomial curve fitting. Richert and Wednt [17] used a two-dimensional Taylor expansion of the calibration map. Wenger [18] utilized look-up error tables for calibrating seven hole pressure probes. This involved adding an extra step to the traditional calibration methods for interpolation of the error look-up tables. A global surface is fitted to the data in order to reduce the magnitude of interpolated parts of the calibration in this method. Then, a local interpolation of lower order polynomial fitting was utilized. This process minimizes the potential for error associated with oscillation in the interpolation function in between the calibration points. Milanovic [19] introduced a numerical calibration method for probes in supersonic flows. Curve fitting and direct interpolation techniques were compared by Sumner [20]. He concluded that both methods showed the same level of accuracy. Pisasale [21] investigated the probe tip geometries and used the potential flow theory around the tip to extend the calibration range. Yasa [22] introduced new calibration coefficients and a robust regression technique to use the complete calibration data for data reduction. These coefficients are not based on differential pressure differences from the opposite ports. Thus, the method can be still effective even if one of the pressure ports are clogged. However, the data reduction and calibration times are considerably longer than the traditional methods due to the iterative process of comparing calibration coefficients from each measurement point to the whole calibration data-set.

Machine learning (ML) techniques can be used to establish the mapping function between the pressure coefficients and flow properties of interests to address some of the shortcomings of the more established calibration and data reduction techniques. Baskaran et al. [23] used neural networks to establish a nonlinear mapping from an input space of experimentally measured differential pressure coefficients to an output space of flow angles, total, and static pressures. Probabilistic Neural Networks (PNN) and Multi-Layer Feed-forward Neural Networks (MLFNN) were utilized to define the mapping function. Prediction uncertainties up to 33% were reported by the authors for the proposed neural networks. The variation of the calibration map with Mach number was neglected by the authors. Soltani et al. [24] proposed using the feed-forward General Regression Neural Networks (GRNN) in order to define the mapping function between normalized pressure coefficients and the flow properties of interest. The calibration method utilized two separate sets of coefficients to perform calibration for flow with low- and high-angle regimes. The prediction uncertainties reported for pitch and yaw were in order of 0.12^o in the range of calibration from 0^o to 65^o. The prediction uncertainty reported for roll angle was 0.17^o. Such low levels of prediction uncertainties were expected for large calibration data-set with neglecting the variation of calibration with Mach number. Rediniotis [25] proposed an approach using Artificial Neural Networks in calibration of multi-hole probes. However, this method suffers from low convergence speeds and the unavoidable local minima in the process of learning for the ANNs. Momentum learning was proposed by the authors to avoid this shortcoming. The adaptive learning method was utilized to increase the speed of convergence in this work. Prediction uncertainty of up to 0.7^o was reported for angular predictions at a specific Mach number. Prediction uncertainty of up to 1.4% for velocity was reported in their work. The authors did not specify the range of velocities considered in training the ANNs for their work. The maximum speed noted in the experimental facility for calibration was reported as $45.7\,m/s$, which avoids the complexity of calibration in the compressible

flow regime. Fan [26] used Differential Evolution Algorithm to address the shortcomings faced by Rediniotis [25]. Acceptable averaged prediction uncertainty of 0.7^o for flow angles was reported, although limited to a specific Mach number. Lee [27] utilized the Adaptive Network-based Fuzzy Inference System (ANFIS) to determine the calibration mapping for five hole probes. ANFIS can be considered as a middle ground technique between neural network and qualitative fuzzy models. Prediction uncertainty for flow angles in the order of 0.007^o for a specific flow Mach number was reported.

The aim of this work is to establish a general framework for using the Artificial Neural Networks in the calibration process for multi-hole probes. First, implementation of machine learning techniques in the traditional iterative algorithms was considered. This was used to reduce the number of calibration points required without losing prediction accuracy. A set of new calibration pressure coefficients were introduced to enable training models for predicting Mach number, total pressure, and flow angles directly from the proposed pressure coefficients. This method significantly reduced data reduction times. The methods introduced here are focused on calibrating five-hole probes, however, these models could be extended to any variation of multi-hole probes.

THEORETICAL BACKGROUND

Five-hole probe with conical tip geometry used in this work had five pressure ports on the tip of the probe. One port is located at the center and the other ports are arranged symmetrically on the sides of the cone. Figure 1 shows the arrangement of the pressure ports. Probe calibration for low-angle flow regime was considered. Thus, it is confirmed that the flow stays fully attached over the tip of the probe over the range of yaw and pitch angles.

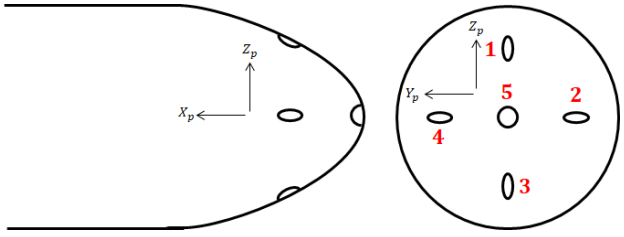

FIGURE 1: NUMBERING SCHEME FOR THE PRESSURE PORTS ON A FIVE HOLE PROBE.

Probe calibration process for the non-nulling technique is to place the probe in a flow with known flow characteristics and then pitch and yaw of the probe were changed to cover a range exceeding the expected flow angles. Each port was connected to a pressure transducer in order to measure absolute pressure values through the calibration process. Calibrations for 12 five-hole probes were obtained in the yaw and pitch angle ranges of $\pm 25^o$ at the NASA Glenn Research Center CE-12, free-jet calibration facility [28]. The straight probes had a conical tip with diameters of 6.35 *mm* or 9.53 *mm*.The probe pressures and the dynamic pressure measurements were performed with Measurement Specialties ESP-HD pressure scanners. The static pressure was monitored with a Omegadyne (209-015A5V) absolute pressure sensor connected to an Omega DP41-E meter. The total temperature was measured with a ITHP-5 probe with an iSeries Humidity and Temperature Controller (DPiTH-I1D-5-C4EI).

The step size of 1^o was used for the range of 0^o to $\pm 4^o$ for both angles. The step size was then increased to 2^o for the range of $\pm 4^o$ to $\pm 9^o$. Finally, the step size of 5^o was used for the rest of the calibration range. Thus, a 19×19 matrix of calibration data was generated for each Mach number as shown in figure 2. The dots refer to the points where calibration data were recorded. This procedure was performed at six different Mach number values of 0.1, 0.2, 0.3, 0.4, 0.5, and 0.6. This brings the total number of calibration data points acquired for each probe to 2166.

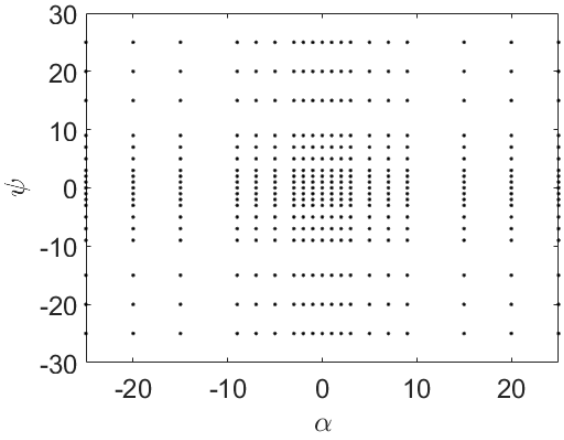

FIGURE 2: MAP OF YAW AND PITCH ANGLES USED FOR GENERATING THE CALIBRATION MAP.

Based on the total pressure, local Mach number, yaw, and pitch angles, the velocity vector can be fully characterized as shown below.

$$\begin{aligned} u &= V \times cos(\alpha) cos(\psi)\, \hat{i}, \\ v &= V \times sin(\alpha)\, \hat{j}, \\ w &= V \times sin(\alpha) cos(\psi)\, \hat{k}. \end{aligned} \tag{1}$$

Where u, v, and w are the velocity components with respect to the coordinate system shown in figure 3, and $\hat{i}$, $\hat{j}$, and $\hat{k}$ are the unit vectors for x, y, and z in the coordinate system.

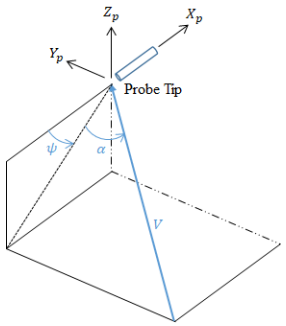

FIGURE 3: DEFINITIONS OF PROBE COORDINATE SYSTEM AND RELATIVE FLOW ANGLES.

For each calibration point, a set of calibration coefficients was calculated from the five pressure port measurements. The most common non-dimensional coefficients are based on differential pressures and defined as [2]

$$P_a = \frac{1}{4}\left(P_1 + P_2 + P_3 + P_4\right), \tag{2}$$

$$cp_\alpha = \frac{P_4 - P_2}{P_5 - P_a}, \qquad cp_\psi = \frac{P_3 - P_1}{P_5 - P_a}, \tag{3}$$

$$cp_t = \frac{P_5 - P_s}{P_t - P_s}, \qquad cp_a = \frac{P_a - P_5}{P_t - P_s}. \tag{4}$$

Where P_1 to P_5 are the pressure readings from the corresponding pressure ports of the five-hole probe, P_t is the local stagnation (total) pressure, and P_s is the local static pressure. For each couple of yaw and pitch, there exists a unique set of calibration coefficients. These non-dimensional coefficients are usually presented by calibration maps [14]. It is inferred that yaw and pitch can be defined by the coupled angular coefficients, (cp_α, cp_ψ) and there is a unique set of cp_t and cp_a for a coupled set of (α, ψ).

The data reduction algorithm [22] can be inferred from the above explanation. When reducing data to determine the variables of interest e.g. total pressure, velocity magnitude, and direction of the flow, only the five pressure values measured during the data acquisition are known. These five pressures can be used to directly calculate cp_α, and cp_ψ. Based on an initial guess for Mach number, the appropriate calibration map can be used to interpolate flow angles α and ψ from (cp_α, cp_ψ). The pressure coefficients (cp_t, cp_a) then can be interpolated using (α, psi). A new Mach number, Ma_{new} can be calculated using the total and static pressure values derived from the corresponding pressure coefficients. The new Mach number is then compared to the initial guess. If a specific threshold is met (e.g. $|Ma_{new} - Ma| < \varepsilon_{Ma}$) then the measurement is complete. Otherwise Ma_{new} will be used as the initial guess for the next iteration.

The robust pressure coefficients introduced by Yasa et al. [22] were of interest to this work. These coefficients were defined as

$$cp_{r1} = \frac{P_1 - P_s}{P_5 - P_s}, \qquad cp_{r2} = \frac{P_2 - P_s}{P_5 - P_s}, \tag{5}$$

$$cp_{r3} = \frac{P_3 - P_s}{P_5 - P_s}, \qquad cp_{r4} = \frac{P_4 - P_s}{P_5 - P_s}, \tag{6}$$

$$cp_t = \frac{P_5 - P_s}{P_t - P_s}, \qquad cp_a = \frac{P_a - P_5}{P_t - P_s}. \tag{7}$$

Yasa et al. utilized the coefficients to build a data base which can be compared to measurement points during the data reduction process through regression methods. The basis of this approach was promising for implementation with machine learning algorithms as it constructed an input space with more variables compared to the traditional methods.

NUMERICAL PROCEDURE

An artificial neural network model was implemented using PyTorch. The number of inputs was set to 5 with each input representing a non-dimensional pressure coefficient. Figure 4 shows an example of the structure of the neural network. Blue circles represent the input vector, the gray circles show the number of neurons arranged per layer, and the green circles represent the outputs of the model. Network inputs are multiplied by the first layer's weight (ω) to create an output Y. The weight matrix and output are then passed into an activation function. The activation function, rectified linear units (relu6) [29], takes the sum of all the weights for a given neuron and if the sum is negative, the neuron is inactive; however, if it is positive then it is active and its value is equal to the value of the input. This can lead to the model diverging which is why relu6 was chosen. Instead

of the value of the neuron being equal to potentially infinity, the limit is capped to 6. The output of the layer combined with the activation function is then passed into the next layer and the activation function. The weights of each layer was optimized using the Adaptive Moment Estimation algorithm (Adam) [30]. The Adam algorithm uses a first order gradient based optimization based on estimates of lower order moments. Optimization was performed for a total of 1000 epochs to ensure convergence.

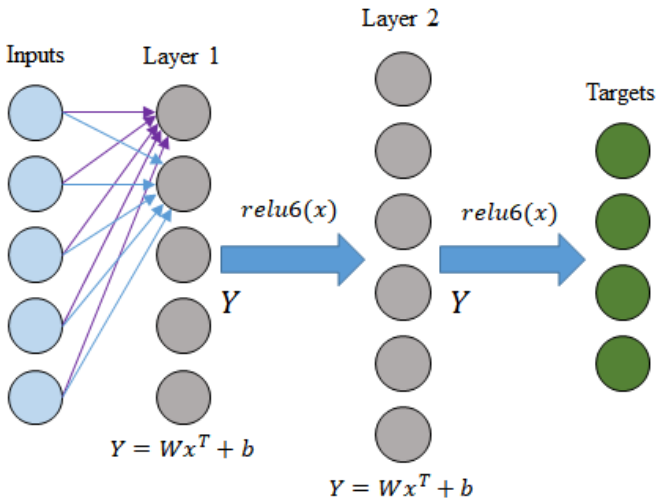

FIGURE 4: SCHEMATIC OF AN ARTIFICIAL NEURAL NETWORK.

Probe flow angles of pitch and yaw were taken for Mach numbers of 0.1 to 0.6 in 0.1 increments. Data was partitioned into *test*, *train*, and *validation* datasets. The *validation* data set is at Mach 0.6; the rest of the data was used as the testing data set. The root-mean squared error between the prediction of the model and the *validation* data set was used in order to validate the trained model. This can be written for a specific trained model as

$$MSE = \sqrt{\frac{1}{N}\sum_{n=1}^{n=N}\left(\mathbb{X}_{Ma=0.5} - \mathbb{X}_{model,Ma=0.5}\right)}. \tag{8}$$

Where, $\mathbb{X}_{Ma=0.6}$ is a feature vector from the *validation* dataset (e.g. cp_t, Ma, etc.), $\mathbb{X}_{model,Ma=0.6}$ is the same feature vector predicted by the trained model, and N is the total number of elements in vector $\mathbb{X}$. Training and test data partition was randomized and then split 70% for training and 30% for testing. All the variables of interest for training ANNs were normalized to values between $[0,1]$ as

$$\mathbb{X}_n = \frac{\mathbb{X} - min\,(\mathbb{X})}{max\,(\mathbb{X}) - min\,(\mathbb{X})}. \tag{9}$$

Where $\mathbb{X}$ is a given feature vector, $\mathbb{X}_n$ is the normalized vector for $\mathbb{X}$, and *min* and *max* are the minimum and maximum values of the feature $\mathbb{X}$, respectively.

For the ANN approach, the numbers of layers (n_L) and neurons per layer (n_N) were allowed to vary. In this study, we constructed 16 cases with different combinations of n_L and n_N. n_L varies from 2 to 16 incrementing $2n$ by ranging n from 1 to 4, and n_N varies from 128 to 1024 in increments of $2n$. Each model was then evaluated for uncertainty with a multiplicative noise based on the assumption that the error is proportional to the pressure measurement. The error is modeled here as a Gaussian with zero mean and variance. Four noise levels (i.e., variance) were analyzed 0, 2.5%, 5% and 10%, and 100 trials for each level was computed. The mean squared error (8) was used to evaluate the sensitivity of the model to noise and it was the criteria for the model comparison.

Model comparison and selection is not trivial when a model is subject to uncertainties.The cost function built in Python module was minimized in using the ANN method mapping input parameters to output parameters. For instance, one of the easiest loss functions is the squared error function defined by

$$Error = \frac{1}{2}(X-D)^{-1}\Gamma^{-1}(X-D), \tag{10}$$

where $D, X \in \mathbb{R}^{N_d}$ is the data and the computed model output, $\Gamma \in \mathbb{R}^{N_d \times N_d}$ is a covariance matrix, which still needs to be specified, and N_d indicates the number of data points. The covariance matrix constitutes a key ingredient in Equation 11, directly influencing the results of the calibration. One possible choice, for instance, is for the covariance matrix to be diagonal which for the sum-of-squares error (SSE), the diagonal component is simply $1/N^d$. Although SSE is a very common way of evaluating the error of a machine learning, this choice is valid only when the data and error are statistically independent. In reality, it is seldom the case. One of simple examples showing dependence among data points is a dynamic problem, where the data point at the current time and the one at the previous time are strongly correlated to each other. Also, a systematic error during the measurements can result in strong dependence among the data points. More complex covariance matrix (cost function) can be used, however it is not easy to do so without a prior knowledge of the uncertainties. In addition, when the cost function in ANN is minimized, weight values need to be updated such that the cost is decreased. To this aim, the derivative of the cost function with respect to each

weight (i.e., Eq. 11) has to be differentiable to update weights, ω.

Uncertainties can be roughly divided into two categories: measurement errors (${\sigma_{exp}}^2$) and physical model inadequacies (${\sigma_p}^2$). For example, the measurement errors in this study include uncertainties in pressure measurements, experimental settings as well as data reduction process, through which experimental raw data provided by measuring instruments are converted into meaningful physical quantities. The model inadequacies are related to uncertainties associated with the surrogate or physical model where uncertain parameters such as the weights in ANN are present. Since these errors are indistinguishable without prior information of one of them, what is observed in Eq. 11 (σ^2) is the sum of these two errors, ${\sigma_{total}}^2 = {\sigma_p}^2 + {\sigma_{exp}}^2$.

Measurement errors and simplifications in the physical model lead to very different performance of the surrogate model in order to capture the true physics and the underlying errors. Therefore, it is important for modelers to decide a metric in order to determine which model is *good*. There are several methodologies of model comparison and selection such as Bayesian information criterion [31–33], deviance information criterion [34–36]. The fundamental idea of model comparison or selection is as follows. To perform model assessment, it is important to handle trade-off between its data-fit (*goodness* to the *fit*) and complexity in order to avoid the extremes of *overfitting* or *underfittin* the data. The second part states how much the model can learn with the data (so-called *information gain*). Therefore, the model performance should be evaluated by [37]

$$\begin{aligned} Model\,Performance(Evidence) = \\ Goodness\,to\,the\,Fit - Information\,Gain. \end{aligned} \tag{11}$$

When it comes to the ANN approach, one of the most powerful features of the ANN is its flexibility such that it makes it possible to model any continuous function linear or nonlinear to an arbitrary degree of accuracy. According to the above equation, ANN shows indeed excellent performance in terms of *Goodness to the fit*. However, despite this powerful feature of ANN, it is still difficult to maximize the model performance by carefully minimizing the model complexity (reducing the *information gain*). The model complexity in ANN is primarily related to selecting the appropriate number of hidden layer nodes, which determines the number of free parameters, weights. Therefore, the goal is to minimize the hidden nodes without losing necessary degree of freedom of the model to accurately capture the true physics and the underlying errors. It is worth noting that ANN with many hidden nodes can suffer from poor calibration of the model parameter when the amount of data is limited or the amount of data is enough, however the information extracted from the data is not sufficient for calibrating all parameters so that the resulting predictions might have a large degree of uncertainty. To this aim, we would like to propose a simple methodology, by which we can evaluate *robustness* of each model in the framework of ANN, instead of numerically calculating the evidence, which is outside of the scope of the current study.

Implementing ML in Existing Algorithms

The existing data reduction algorithms which do not utilize the machine learning techniques can be divided in two general categories. The *traditional* algorithms and the regression algorithms as the one proposed by Yasa (*robust* algorithm [22]). The *traditional* method iterates over the local Mach number value while the *robust* method iterates over the local static pressure. The *traditional* algorithm has two interpolation steps as explained before which can be substituted by trained artificial neural network models. The procedure for implementing this ML method in the *traditional* algorithm is shown in Fig. 5. The shortcoming of this method aside from the long iterative process is the need of large calibration data-sets. Since this calibration is based on the differential pressure measurements, it cannot be used if one of the pressure ports on the probe is completely or slightly clogged due to the conditions at the experimental facility (i.e. icing, condensation, impurities in the flow).

The flow angles α and ψ were used as targets with the angular coefficients cp_α and cp_ψ as inputs to train the ANN model, $\mathbb{M}_1$. The second ANN model, $\mathbb{M}_2$ is trained with cp_t and cp_a as targets and α and ψ as inputs. During the data reduction, the angular coefficients are calculated based on the experimental measurements. Flow angles are then calculated using model $\mathbb{M}_1$ and the flow angles as inputs. The outputs from model $\mathbb{M}_1$ form the inputs for the second model $\mathbb{M}_2$ to compute the two remaining pressure coefficients, cp_t and cp_a. The rest of the iterative algorithm is similar to the *traditional* algorithm.

In the *robust* data reduction method, none of the calibration coefficients can be calculated directly from the measurements. Thus the process starts from an initial guess for the static pressure, which is required to calculate the primary pressure coefficients cp_{r1} to cp_{r4}. For each measurement time window, the resulting non-dimensional values of pressure are compared, one by one, to the corresponding values in the database. The comparison is evaluated through a regression coefficient, which approaches unity when the probe readings agree with the calibration data-set. A polynomial surface fit is then used to find the values for flow angles α, and ψ. The remaining coefficients, cp_t and cp_a will then be interpolated to calculate total pressure, static pressure, and Mach number. If the difference between the new static pressure and the initial guess is below some threshold, the iteration will stop. Otherwise, the new static pressure value will be used to recalculate cp_1 to cp_4. This procedure needs a relatively large calibration data-set and extremely long data processing times. The regression process can be replaced by the trained Artificial

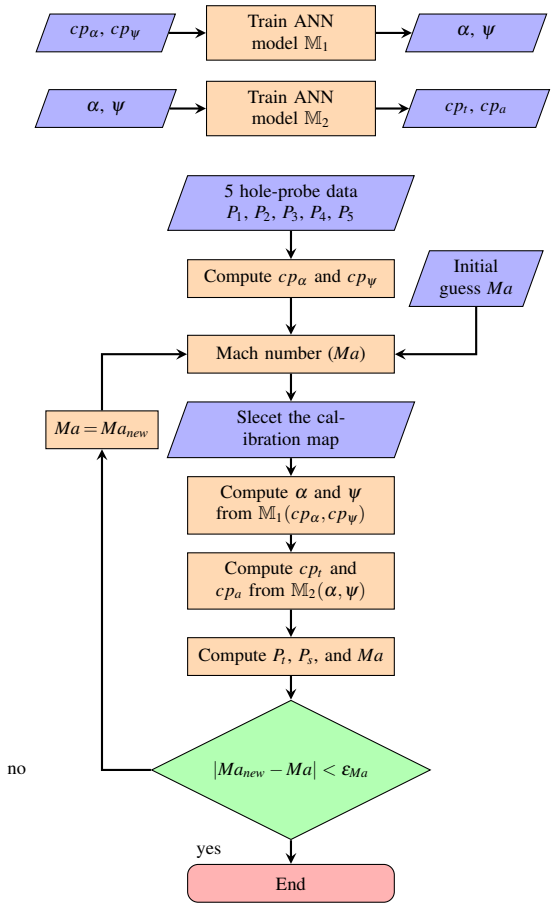

FIGURE 5: IMPLEMENTATION OF ML METHOD IN DATA REDUCTION ALGORITHM FOR THE TRADITIONAL CALIBRATION METHOD

Neural Networks as shown in figure 6 to significantly reduce the processing time.

Two ANN models were trained using the calibration coefficients cp_{r1} to cp_{r4} as inputs. Flow angles were used as targets for $\mathbb{M}_1$. Pressure coefficients cp_t and cp_a were used as targets for the second model, $\mathbb{M}_2$. The algorithm after this step is similar to what was described for the *robust* data reduction algorithm. It is of importance to note that a single model can be constructed to map calibration coefficients cp_{r1} to cp_{r4} to the four outputs of interest however, the prediction uncertainties were significantly increased in this method.

ML Friendly Algorithm

Implementing machine learning methods in the previously proposed calibration methods were limited to tools for surface fitting due to the iterative nature of these techniques. In order to fully take advantage of the flexibility of deep learning for ANNs,

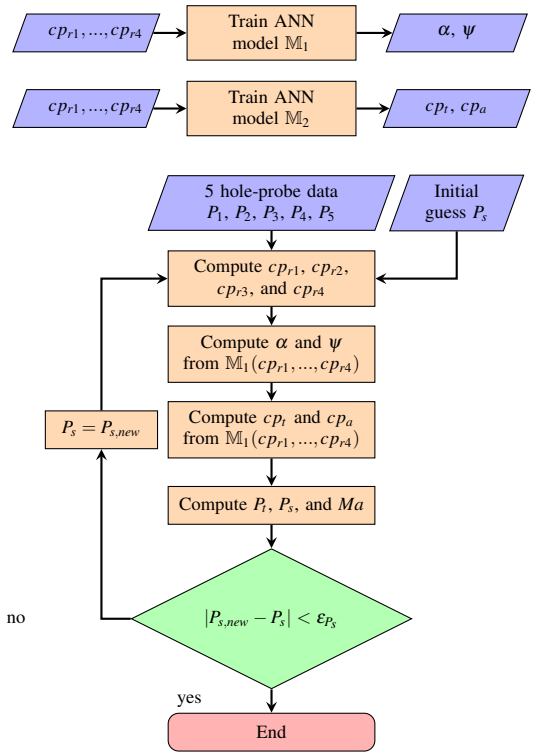

FIGURE 6: DATA REDUCTION ALGORITHM FOR THE *ROBUST* CALIBRATION METHOD

a new set of coefficients are introduced as

$$cp_1 = \frac{P_1 - P_a}{P_5 - P_a}, \qquad cp_2 = \frac{P_2 - P_a}{P_5 - P_a}, \tag{12}$$

$$cp_3 = \frac{P_3 - P_a}{P_5 - P_a}, \qquad cp_4 = \frac{P_4 - P_a}{P_5 - P_a}, \tag{13}$$

$$cp_t = \frac{P_5 - P_s}{P_t - P_s}, \qquad cp_m = \frac{P_5 - P_a}{P_5}. \tag{14}$$

The coefficients, cp_1 to cp_4 are similar to the robust calibration coefficients cp_{r1} to cp_{r4} with the difference that the proposed set of coefficients are calculated with P_a, instead of P_s. Thus, these coefficients can be calculated directly for the data reduction purposes without the need for an initial guessing of local flow properties. These four coefficients build up an input space for an ANN with more degrees of freedom to provide a better fit

to the data. The total pressure coefficient, cp_t is similar across the different methods introduced here. The sixth coefficient, cp_m is representative of the flow Mach number, which can also be calculated directly. During the data reduction process, cp_m limits the results to a specific Mach number and then the quantities of interest can be specified by the remaining coefficients for that Mach number.

Variation of the calibration coefficients with the flow angles are shown in Fig. 7. Each coefficient reaches its maximum value when its corresponding port is aligned with the direction of the flow. However, when the opposite pressure tap is positioned in the flow direction, the port of interest resides in the wake of the probe tip. Consequently, it registers lower pressure values, causing the respective pressure coefficient to approach its minimum value.

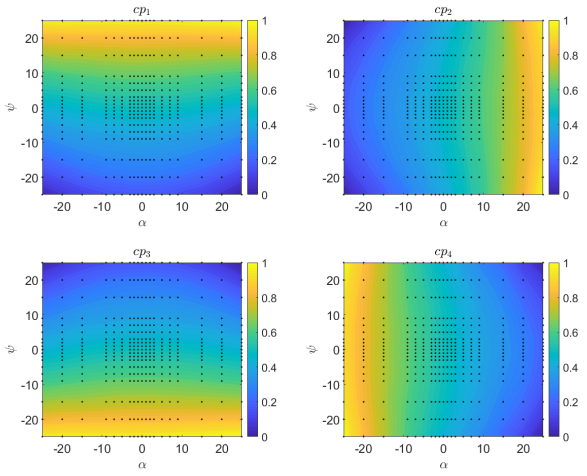

FIGURE 7: VARIATION OF PROPOSED CALIBRATION COEFFICIENTS cp_1 (TOP LEFT), cp_2 (TOP RIGHT), cp_3 (BOTTOM LEFT), AND cp_4 (BOTTOM RIGHT) WITH FLOW ANGLES.

Figure 8 shows the variation of cp_m with flow Mach number for the complete calibration data-set of a single five hole probe with 2166 calibration points. The calibration coefficient, cp_m is shown on the abscissa and the ordinate shows the flow Mach number. The experimental data are shown on the plot as cluster of points. This figure clearly represents the separation of cp_m with Mach number, which can be utilized in training the ANN model.

The model training and data reduction algorithms are laid out in Fig. 9. Five calibration coefficients, cp_1, cp_2, cp_3, cp_4, and cp_m were used as inputs to train two ANN models. The

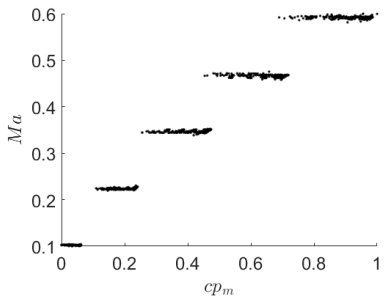

FIGURE 8: VARIATION OF cp_m WITH FLOW MACH NUMBER.

model $\mathbb{M}_1$ used the flow angles α and ψ as targets while the second model $\mathbb{M}_2$ was trained with the total pressure coefficient and Mach number as targets. These two models then can be directly utilized for data reduction purpose. The aforementioned calibration coefficients can be directly calculated from the experimental measurements. The trained models would use the inputs to compute the values of interest with no need for an iterative algorithm.

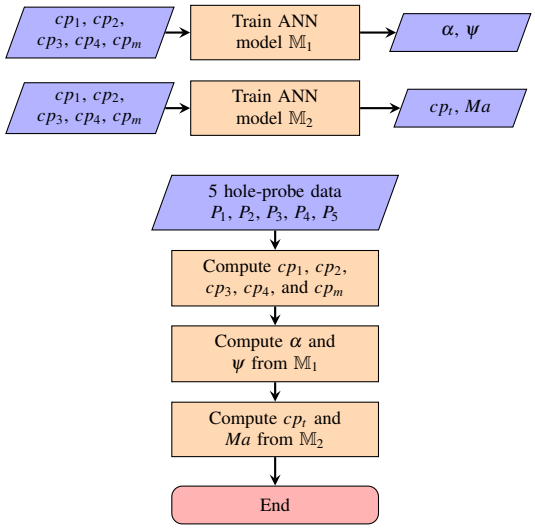

FIGURE 9: DATA REDUCTION ALGORITHM WITH UTILIZING ML FRIENDLY CALIBRATION COEFFICIENTS.

If pressure measurement from one of the pressure ports is unavailable, there is sufficient distinction among the values of the proposed calibration coefficients to allow an effective new calibration utilizing the remaining coefficients. For instance if pressure port 1 is inaccessible, the model $\mathbb{M}_1\,(cp_1, cp_2, cp_3, cp_4, cp_m)$ can be retrained as $\mathbb{M}_{1p}\,(cp_2, cp_3, cp_4, cp_m)$ to compute the properties of interest

with an acceptable uncertainty. A loss of no more than 1% in prediction uncertainty for properties of interest was noticed by eliminating one of the pressure coefficients except cp_m. Loss of cp_m means loss of pressure reading from port 5 and since all the coefficients are tied to port 5, this methodology is fruitless if that port is lost.

RESULTS

One of the main goals of this study was to show that by using ML methods, the number of calibration points can be decreased while maintaining the prediction accuracy. The original 19×19 matrix of data (see Fig. 2 for a given Mach number was reduced to 12×12 matrix as shown in Fig. 10. The black dots show the complete set of pitch and yaw angles used in the calibration of the five-hole probe. The calibration points that were used for assessing implementation of ML in the traditional algorithm are marked with red circles.

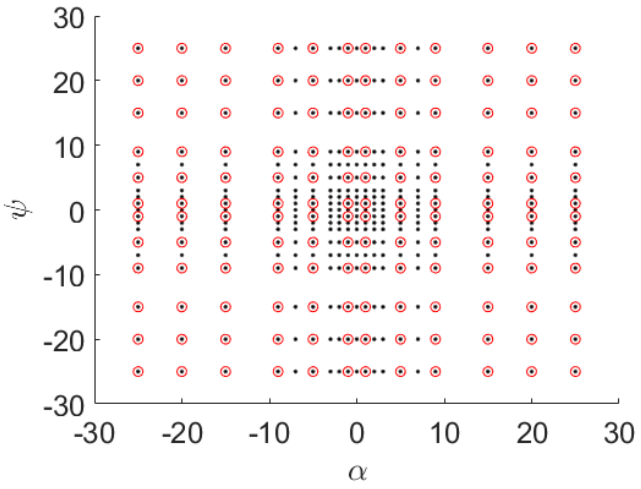

FIGURE 10: MODIFIED CALIBRATION MAP

In order to asses this in the traditional calibration method two separate ANNs were constructed. This was performed for Mach number of 0.6 which had the most complexity in the calibration. The higher the Mach number, the higher is the Reynolds number which may cause worst flow separation and vortex shedding. This is previously investigated by Crawford [38]. Since both ANNs were constructed with similar structure and both have two input vectors and two output vectors, they showed overall similar uncertainties. Here the results for $\mathbb{M}_1$ are discussed in detail. The ANN had one output layer and n_H hidden layers which were varied to obtain the minimum root mean squared error between the testing and training data-sets. The training data-set consisted of the calibration data marked with the red circle. The testing data-set was the complete calibration data shown with the black dots. The trained ANN model was used to replace surface fitting methods thus its effectiveness can be evaluated by the mean squared error (see equation 8) between the predictions and the experimental calibration data.

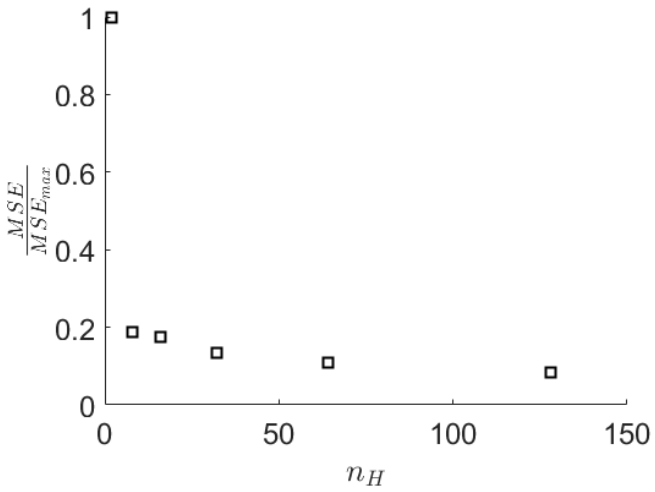

FIGURE 11: THE VARIATION OF OVERALL NORMALIZED MSE IN FLOW ANGLE PREDICTION WITH NUMBER OF HIDDEN LAYERS AT MACH NUMBER OF 0.6.

Uncertainty in angular prediction versus number of hidden layers is shown in figure 11. The MSE decreased by 80% by choosing 8 hidden layers compared to 2 hidden layers and does not significantly change as n_H was increased to 128. Thus, ANN architecture with16 hidden layers and 10 neurons in each layer was chosen for constructing $\mathbb{M}_1$. The averaged MSE percentage for predicting yaw and pitch was 0.12% over the $50\,deg.$ range of flow angles during calibration. The averaged MSE percentage for predicting cp_a and cp_t were 0.21% and 0.09% respectively. It can be directly inferred from the prediction uncertainties that reducing the number of calibration points did not significantly reduce the prediction uncertainty of the trained ANNs. This is better shown by investigating percentage MSE in predicting yaw angle with $\mathbb{M}_1$ in figure 12. In this figure the contour of MSE is shown versus the pitch and yaw calibration coefficients. There are local maximas for MSE which do not exceed 1% error.

The same approach can be taken in constructing the two ANN models for robust algorithm described in Fig. 6. These models had similar properties and the averaged MSE can be utilized to evaluate the acceptable number of hidden layer. Figure

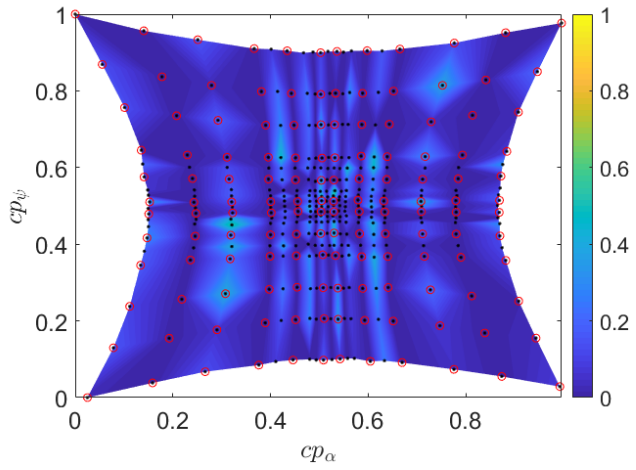

FIGURE 12: THE PERCENTAGE OF ROOT MEAN SQUARED ERROR FOR PREDICTING YAW WITH AN ANN AT MACH NUMBER OF 0.6 IN TRADITIONAL ALGORITHM.

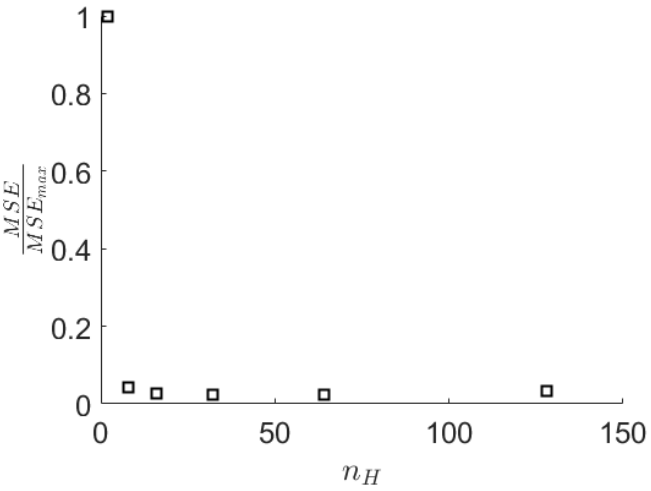

FIGURE 13: THE PERCENTAGE OF ROOT MEAN SQUARED ERROR FOR PREDICTING YAW WITH AN ANN AT MACH NUMBER OF 0.6 IN YASA ET. AL'S ROBUST ALGORITHM.

13 shows the average overall MSE in predicting flow angles with $\mathbb{M}_1$ for implementing ML methods in the robust calibration algorithm. Sixteen hidden layers were chosen for constructing the models. They were trained with the reduced 12×12 calibration matrix at Mach number of 0.6. The models predictions were compared to the complete calibration data set to report the uncertainty values. The averaged percentage MSE for predicting yaw and pitch was 0.03% over the $50\,deg.$ range of flow angles during calibration. The averaged percentage MSE for predicting cp_a and cp_t were 0.2% and 0.14% respectively.

Lastly, similar approach was taken in choosing the number of hidden layers for using the proposed ML friendly algorithm described in Figure 9. Two ANN models with 16 hidden layers were constructed with each layer containing 10 neurons. The reduced data-set matrix for all the available Mach numbers were used to train the models $\mathbb{M}_1$ and $\mathbb{M}_2$. The uncertainties were calculated using the models on the full calibration data set. The averaged percentage MSE for predicting yaw and pitch was 0.11% over the $50\,deg.$ range of flow angles during calibration. The averaged percentage MSE for predicting cp_m and Mach number were 0.23% and 0.37% respectively. Figures 14 and 15 show the percentage MSE for flow angles and Mach number receptively, based on the complete calibration dataset of a single five-hole probe. This method provides a very robust algorithm for calibrating five-hole probes which can be extended to any multi-hole probe.

This approach has been demonstrated to yield highly accurate results, with processing times typically taking only a few seconds in contrast with the robust method which had maximum processing times of about 15 minutes for the same data set. Although the traditional calibration method boasts a comparable processing time, it necessitates 2.5 times more data points to achieve the same level of uncertainty as the ML-friendly algorithm. This method enables a reduction in calibration time and associated costs by nearly 60%.

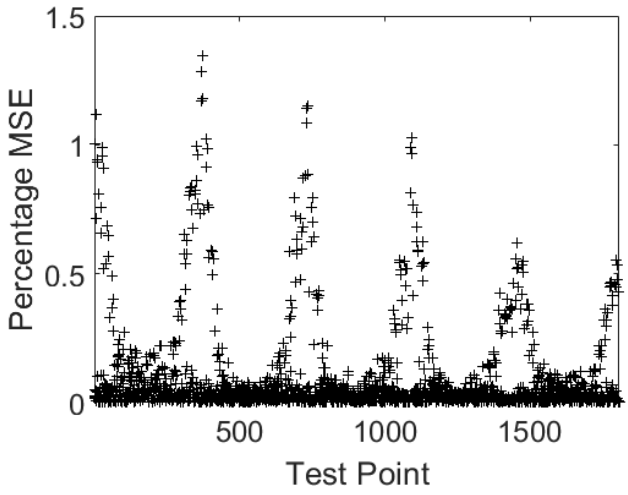

FIGURE 14: THE AVERAGED PERCENTAGE OF ROOT MEAN SQUARED ERROR FOR PREDICTING FLOW MACH NUMBER USING ML FRIENDLY ALGORITHM.

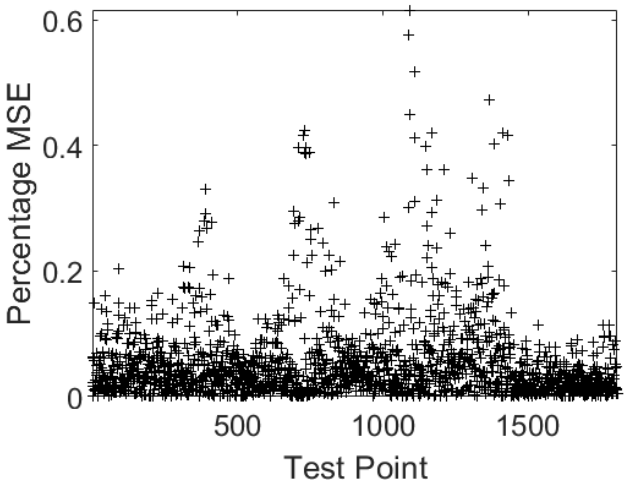

FIGURE 15: THE AVERAGED PERCENTAGE OF ROOT MEAN SQUARED ERROR FOR PREDICTING FLOW ANGLES USING ML FRIENDLY ALGORITHM.

A simple methodology to investigate the *robustness* of the trained model is proposed. The cost function implemented in PyTorch was used assuming that all training data points are statistically independent. it is natural to assume that the pressure measurements also have statistically independent noise . There could be a systematic error during the measurement, causing some data points to be strongly correlated, however this type of error is not considered in this study and left for future studies. There are many possible error structures such as additive noise, multiplicative noise. For instance, an additive noise is based on the assumption that the error is independent from the measured value and can be expressed by $D_i' = D_i + \varepsilon$, where D_i is the ith experimental data, and $\varepsilon = X_i - D_i'$ represents the sum of the experimental uncertainty and error in the physical model. ε could be expressed by the Gaussian white noise given the mean and the variance. A multiplicative noise, which assumes that the noise level is proportional to the value of the measurement, is described by $D_i' = D_i \times exp(\varepsilon)$. Note that if the log of X_i and D_i is taken, the error $\varepsilon = log(X_i) - log(D_i')$ follows the Gaussian white noise. There is no information about the sources of errors in this measurement, thus it is impossible to determine which error structures are more relevant to this measurement. However, a simple test can be performed to examine the robustness of the trained model when using the data with a pre-described noise level. To this aim, only a multiplicative noise for the rest of this study was taken into account.

For a given noise level, the number of neurons were varied between 1 to 100 and the number of layers were varied between 1 and 16. The averaged MSE for 100 trials of training ANNs with the aforementioned criteria as explained in section were studied. Figure 16 show the contour plots of the mean squared error (MSE) for four different noise levels, (a) 0.0, (b) 0.025, (c) 0.05, and (d) 0.1 over a large parameter space of the number of neurons (n_n) and layers (n_h) used in the ANN method explained in section refsec:NPro. All data were averaged over 100 trials. There are several key features that may be observed. MSE became independent from n_n when N_L became small. For instance, in the case of noise level =0.0 (see Fig. 16a), MSE is less than 0.05 regardless of n_n. This observation implies that the model was capable of predicting the data well with a relatively low degree of freedom of the model parameters.When n_h was more than 500, we observed the dependency of MSE on both n_n and n_h. In fact, the maximum values of MSE appear for the large number of $n_h = 1024$ and the relatively small number of n_h (4 for the low level of noise and 8 for the high level of noise). Considering that the degree of freedom of the model might be estimated by the product of n_n and n_h. For all cases, MSE remains small when $n_n = 2$. For this particular model, the model with $n_n = 2$ is more tolerant against the overfitting problem with the increase of n_h. The maximum and minimum values of MSE increase as the noise level increases (for instance, $\text{MSE}_{max} = 0.5$ for the noise level =0.0 and SME_{max} = 1.2 for the noise level =0.1) . This result should help a user understanding how much uncertainty the model can tolerate given the required accuracy. A good model should show a relatively slow increase in the error with the increase of the noise level. Overall, as mentioned before this approach showed great results with $n_h = 16$ and $n_n = 10$ with the understanding that user can investigate the errors and fitting further in a specific calibration case.

CONCLUSION

This study introduced methods to implement machine learning methods in the existing five-hole calibration and data reduction algorithms. ANNs were utilized instead of regular surface fitting techniques in these algorithms. The processing times were reduced significantly by using ANNs in these traditional algorithms while the accuracy was preserved. These techniques were assessed using experimental calibration data for five-hole probes. The method can be extended to any existing multi-hole probe calibration algorithm A set of machine learning friendly calibration coefficients were introduced in this work. These coefficients eliminate the need for iterative algorithms. Thus, flow properties of interest (e.g. Mach number, yaw, pitch, and static and total pressures) can be directly computed by training appropriate ANNS.

ACKNOWLEDGMENT

The authors would like to thank Dr. Julia Stephens, Aaron Johnson, Celia Otero, and Ezra Mcnichols for providing us with

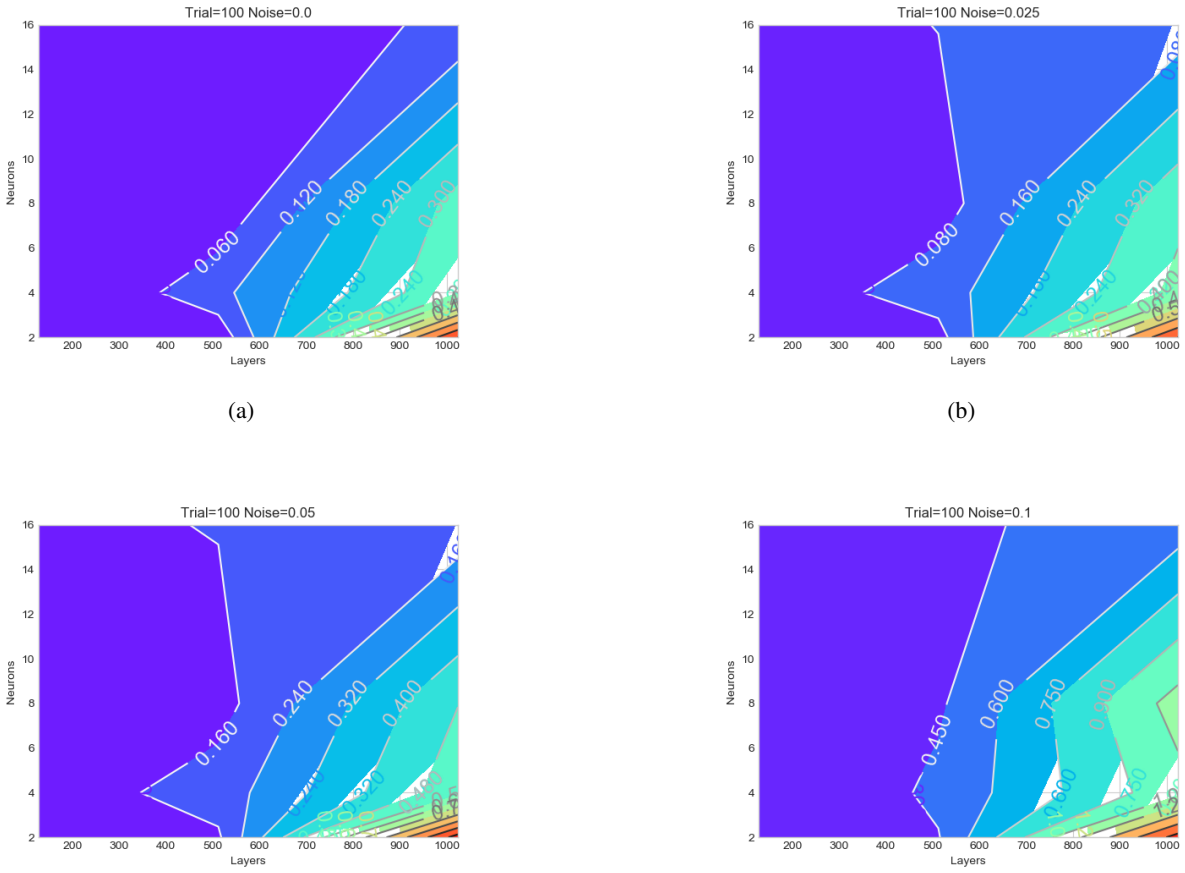

FIGURE 16: MSE contours of ANN models, averaged for 100 trials

the state of the art calibration data used in this research work and for their comments that greatly improved this study.

REFERENCES

[1] Dudzinski, T., and Krause, L. N., 1969. "Flow-direction measurement with fixed-position probes". *National Aeronautics and Space Administration*.

[2] Treaster, A. L., and Yocum, A. M., 1978. *The calibration and application of five-hole probes*. NTIS.

[3] Zilliac, G. G., 1989. Calibration of seven-hole pressure probes for use in fluid flows with large angularity. Tech. Rep. 102200, NASA.

[4] Zilliac, G. G., 1993. "Modelling, calibration, and error analysis of seven-hole pressure probes". *Experiments in Fluids,* ***14***(1-2), pp. 104–120.

[5] Babu, C. V., Govardhan, M., and Sitaram, N., 1998. "A method of calibration of a seven-hole pressure probe for measuring highly three-dimensional flows". *Measurement Science and Technology,* ***9***(3), p. 468.

[6] Pisasale, A. J., and Ahmed, N. A., 2002. "A novel method for extending the calibration range of five-hole probe for highly three-dimensional flows". *Flow Measurement and Instrumentation,* ***13***(1-2), pp. 23–30.

[7] Gossweiler, C. R., Kupferschmied, P., and Gyarmathy, G., 1994. "On fast-response probes: Part 1–technology, calibration and application to turbomachinery". Vol. 78873, American Society of Mechanical Engineers.

[8] Dominy, R. G., and Hodson, H. P., 1992. "An investigation of factors influencing the calibration of 5-hole probes for 3-d flow measurements". Vol. 78934, American Society of Mechanical Engineers.

[9] Johansen, E. S., Rediniotis, O. K., and Jones, G., 2000. "The compressible calibration of miniature multi-hole probes". *J. Fluids Eng.,* ***123***(1), pp. 128–138.

[10] Rediniotis, O. K., and Chrysanthakopoulos, G., 1998. "Ap-

plication of neural networks and fuzzy logic to the calibration of the seven-hole probe". *Journal of fluids engineering,* ***120***(1), pp. 95–101.

[11] Zeiger, M., Chalmeta, L., and Telionis, D., 1998. "Tip geometry effects on calibration and performance of seven-hole probes". p. 2810.

[12] Schaub, U. W., Sharp, C. R., Bassett, R. W., and Schaub, U. W., 1964. An investigation of the three-dimensional-flow characteristics of a non-nulling five-tube probe. Tech. Rep. LR-393, National Research Laboratories, Ottawa, Canada.

[13] Wickens, R. H., and Williams, C. D., 1985. Calibration and use of five-hole flow direction probes for low speed wind tunnel application. Tech. Rep. 24468, National Research Council Canada.

[14] Morrison, G. L., Schobeiri, M. T., and Pappu, K. R., 1998. "Five-hole pressure probe analysis technique". *Flow Measurement and Instrumentation,* ***9***(3), pp. 153–158.

[15] Bryer, D. W., and Pankhurst, R. C., 1971. *Pressure-probe methods for determining wind speed and flow direction*. HMSO.

[16] Gallington, G. G., 1980. "Measurement of very large flow angles with non-nuling seven-hole probes". *Aeronautics Digest, USAFA-TR-80-17*, pp. 60–88.

[17] Reichert, B. A., and Wendt, B. J., 1994. A new algorithm for five-hole probe calibration, data reduction, and uncertainty analysis. Tech. Rep. 106458, NASA.

[18] Wenger, C. W., and Devenport, W. J., 1999. "Seven-hole pressure probe calibration method utilizing look-up error tables". *AIAA journal,* ***37***(6), pp. 675–679.

[19] Milanovic, I. M., and Kalkhoran, I. M., 2000. "Numerical calibration of a conical five-hole probe for supersonic measurements". *Measurement Science and Technology,* ***11***(12), p. 1812.

[20] Sumner, D., 2002. "A comparison of data-reduction methods for a seven-hole probe". *Journal of Fluids Engineering,* ***124***(2), pp. 523–527.

[21] Pisasale, A. J., and Ahmed, N. A., 2002. "Theoretical calibration for highly three-dimensional low-speed flows of a five-hole probe". *Measurement Science and Technology,* ***13***(7), p. 1100.

[22] Yasa, T., and Paniagua, G., 2012. "Robust procedure for multi-hole probe data processing". *Flow Measurement and Instrumentation,* ***26***, pp. 46–54.

[23] Baskaran, S., Ramachandran, N., and Noever, D., 1999. "Probabilistic and other neural nets in multi-hole probe calibration and flow angularity pattern recognition". *Pattern Analysis & Applications,* ***2***(1), pp. 92–98.

[24] Soltani, M., Sadati, N., Masdari, M., and Ghorbani, R., 2002. "Neural network based calibration of a seven-hole probe". In 10th Iranian Conference on Electrical Engineering.

[25] Rediniotis, O. K., and Vijayagopal, R., 1999. "Miniature multihole pressure probes and their neural-network-based calibration". *AIAA journal,* ***37***(6), pp. 666–674.

[26] Fan, H.-Y., Lu, W.-z., Xi, G., and Wang, S.-j., 2003. "An improved neural-network-based calibration method for aerodynamic pressure probes". *J. Fluids Eng.,* ***125***(1), pp. 113–120.

[27] Lee, H.-H., Shinder, I. I., Wright, J. D., and Moldover, M. R., 2014. "Application of anfis method to the non-nulling calibration of multi-hole pitot tube". *Procedia Engineering,* ***79***, pp. 125–132.

[28] Gonsalez, J. C., and Arrington, E. A., 1999. Five-hole flow angle probe calibration for the nasa glenn icing research tunnel. Tech. Rep. CR–1999-202330, NASA.

[29] Doğan, G., and Ergen, B., 2024. "A new hybrid mobile cnn approach for crosswalk recognition in autonomous vehicles". *Multimedia Tools and Applications*, pp. 1–16.

[30] Kingma, D. P., and Ba, J., 2014. "Adam: A method for stochastic optimization". *arXiv preprint arXiv:1412.6980*.

[31] Schwarz, G., 1978. "Estimating the dimension of a model". *The annals of statistics,* ***6***(2), pp. 461–464.

[32] Raftery, A. E., 1995. "Bayesian model selection in social research". *Sociological methodology,* ***25***, pp. 111–164.

[33] Wasserman, L., 2000. "Bayesian model selection and model averaging". *Journal of mathematical psychology,* ***44***(1), pp. 92–107.

[34] Beck, J. L., and Yuen, K.-V., 2004. "Model selection using response measurements: Bayesian probabilistic approach". *Journal of Engineering Mechanics,* ***130***(2), pp. 192–203.

[35] Spiegelhalter, D. J., Best, N. G., Carlin, B. P., and Van Der Linde, A., 2002. "Bayesian measures of model complexity and fit". *Journal of the royal statistical society: Series b (statistical methodology),* ***64***(4), pp. 583–639.

[36] Congdon, P., 2007. *Bayesian statistical modelling*, Vol. 704. John Wiley & Sons.

[37] MacKay, D. J. C., 1995. "Probable networks and plausible predictions–a review of practical bayesian methods for supervised neural networks". *Network: computation in neural systems,* ***6***(3), pp. 469–505.

[38] Crawford, J., 2011. Design and calibration of seven hole probes for flow measurement.